Deposition of playa windblown dust over geologic time scales

Jon D. Pelletier*
Joseph P. Cook
Department of Geosciences, University of Arizona, Gould-Simpson Building, 1040 East Fourth Street, Tucson, Arizona 85721-0077, USA

ABSTRACT

Thick eolian deposits are commonly observed beneath desert pavements downwind of dust-emitting playas. These deposits play an important role in piedmont-surface evolution, controlling surface hydrologic conductivity and rates of pedogenesis. To better understand the factors controlling the spatial distribution of eolian deposition, we developed a numerical model that treats deposition from spatially distributed playa sources using analytic point-source solutions for deposition from a Gaussian plume. The model also accounts for complex downwind topography. As a test case, model predictions were compared to eolian deposit thicknesses on Eagle Mountain piedmont, southern Amargosa Valley, California, which receives dust from nearby Franklin Lake playa. The close relationship between the model predictions and mapped thicknesses suggests that eolian transport and deposition can be modeled from basin to regional scales within this framework. These results have important implications for hydrologic, pedogenic, and air-quality problems.

Keywords: eolian, playa, Quaternary, numerical model, Gaussian plume.

INTRODUCTION

The dust cycle in arid environments is characterized by a net eolian transfer of dust from playas to piedmonts (Pye, 1987). Understanding the processes and rates of this transfer is important for many basic and applied geologic problems. For example, since windblown dust is a human health hazard and a visibility problem (e.g., Samet et al., 2000; Watson, 2002), rates of dust transport must be constrained over geologic time scales to identify significant trends and anthropogenic controls in modern dust records. Climatically, eolian dust contributes to global climate change by modifying Earth's albedo (Harrison et al., 2001). Geomorphically, dust deposition plays a fundamental role in the evolution of piedmont surfaces and soils (Yaalon and Ganor, 1973; McFadden et al., 1987; Reheis et al., 1995; Wells et al., 1995). Hydrologically, eolian deposits control surface conductivity (Yaalon and Ganor, 1973). Predicting recharge pathways to subsurface aquifers therefore requires accurate predictive models for eolian deposition on piedmont surfaces at basin to regional scales over geologic time.

Dust deposition rates exhibit strong variability over a wide range of spatial and temporal scales, reflecting variations in source location, regional topography, climatic change, and other factors. Increased pedogenic rates in the Holocene, for example, are associated with increased aridity and higher dust fluxes (Chadwick and Davis, 1990; Reheis et al., 1995). Spatial variability in dust transport and deposition has also been quantified, but available data are of limited resolution (Reheis et al., 1995; Reheis, 2003). Moreover, although dust transport is inherently a multiscale problem, many aspects of dust research focus on either microscale (e.g., crust formation and disturbance) or macroscale (e.g., global numerical modeling) processes, with few studies aimed squarely at intermediate scales (Kohfeld et al., 2005). Kohfeld et al. recommended bridging this gap by integrating regional-scale numerical modeling and field-based geologic studies. This study adopts that approach with a combination of basin-scale numerical modeling, Quaternary surficial geologic mapping, and field-based measurements to quantify dust deposition at spatial scales ranging from 10^1 to 10^5 m over several Quaternary time scales.

*E-mail: jon@geo.arizona.edu.

FIELD OBSERVATIONS

Our study area is located in southern Amargosa Valley, California, where Franklin Lake playa abuts the Eagle Mountain piedmont (Fig. 1A). The water table in Franklin Lake playa is <3 m below the surface (Czarnecki, 1997). Vapor discharge from this shallow aquifer creates a ''soft, puffy, porous'' surface responsible for unusually high dust fluxes (Czarnecki, 1997, p. 5). Czarnecki identified several distinct geomorphic surfaces on Franklin Lake playa that can be readily identified in LANDSAT imagery (Fig. 1A). For the purposes of numerical modeling, the active portion of the playa was mapped based on Czarnecki's map of playa surfaces with significant dust-emitting potential (Fig. 1A).

The Eagle Mountain piedmont acts as the depositional substrate for dust emitted from Franklin Lake playa under northerly wind conditions (see wind-rose diagram in Fig. 1A). Silt-rich eolian deposits occur directly underneath the desert pavements of Eagle Mountain piedmont, varying in thickness from 0 to 80 cm based on soil-pit measurements (Data Repository Appendix DR1[1]). The technical term for these deposits is cumulic eolian epipedons (McFadden et al., 2005), but we refer to them as eolian or silt layers for simplicity. These layers are predominantly composed of silt but also include some fine sand and soluble salts. The homogeneity of these deposits, combined with their rapid transition to gravelly alluvial fan deposits below, makes the layer thickness a reasonable proxy for the total dust content of the soil.

Alluvial fan terraces on Eagle Mountain piedmont have a range of ages, enabling a temporal as well as a spatial record of dust deposition to be reconstructed. Eagle Mountain piedmont exhibits the classic sequence of Quaternary alluvial fan terraces widely recognized in the southwestern United States (Bull, 1991). This terrace sequence is significant for this study because each surface represents a distinct time interval over which dust has been accumulating. Silt layers were observed on all Eagle Mountain terraces that were late Pleistocene in age or older, with maximum values for each terrace unit located closest to the playa. Mapping and correlation of the units to the regional chronology of Whitney et al. (2004) are described in Appendix DR1.

In this study we focus on silt thicknesses of the Qa3 terrace unit (middle to late Pleistocene) because of its extensive preservation and limited evidence of hillslope erosion. Silt thicknesses were measured at locations with undisturbed planar terrace remnants to the greatest extent possible. Repeat measurements of silt thickness within a local area generally yielded the same values to within 3 cm. A color map of silt layer thickness for this surface (obtained by spherical kriging in ArcGIS 9.0) is shown in Figure 1B, draped over the U.S. Geological Survey 30 m digital elevation model and an orthophotograph of the area. Silt thickness is observed to decrease by a factor of $\sim$2 for every 1 km of distance from the playa. Several kilometers downwind, a background thickness of 15–20 cm was observed on Qa3 surfaces. The strongly localized nature of downwind deposition in this area suggests that Franklin Lake playa is the source for nearly all of the eolian deposition on Eagle Mountain piedmont. Localized deposition also implies that dust deposition rates may vary regionally by an order of magnitude or more, down to spatial scales of 1 km or less, with important implications for desert surface and soil evolution.

Figure 2A illustrates plots of silt thickness as a function of downwind distance, for comparison with two-dimensional model results

[1]GSA Data Repository item 2005177, Appendix DR1, further discussion of dust deposition and field-based measurements, is available online at www.geosociety.org/pubs/ft2005.htm, or on request from editing@geosociety.org or Documents Secretary, GSA, P.O. Box 9140, Boulder, CO 80301-9140, USA.

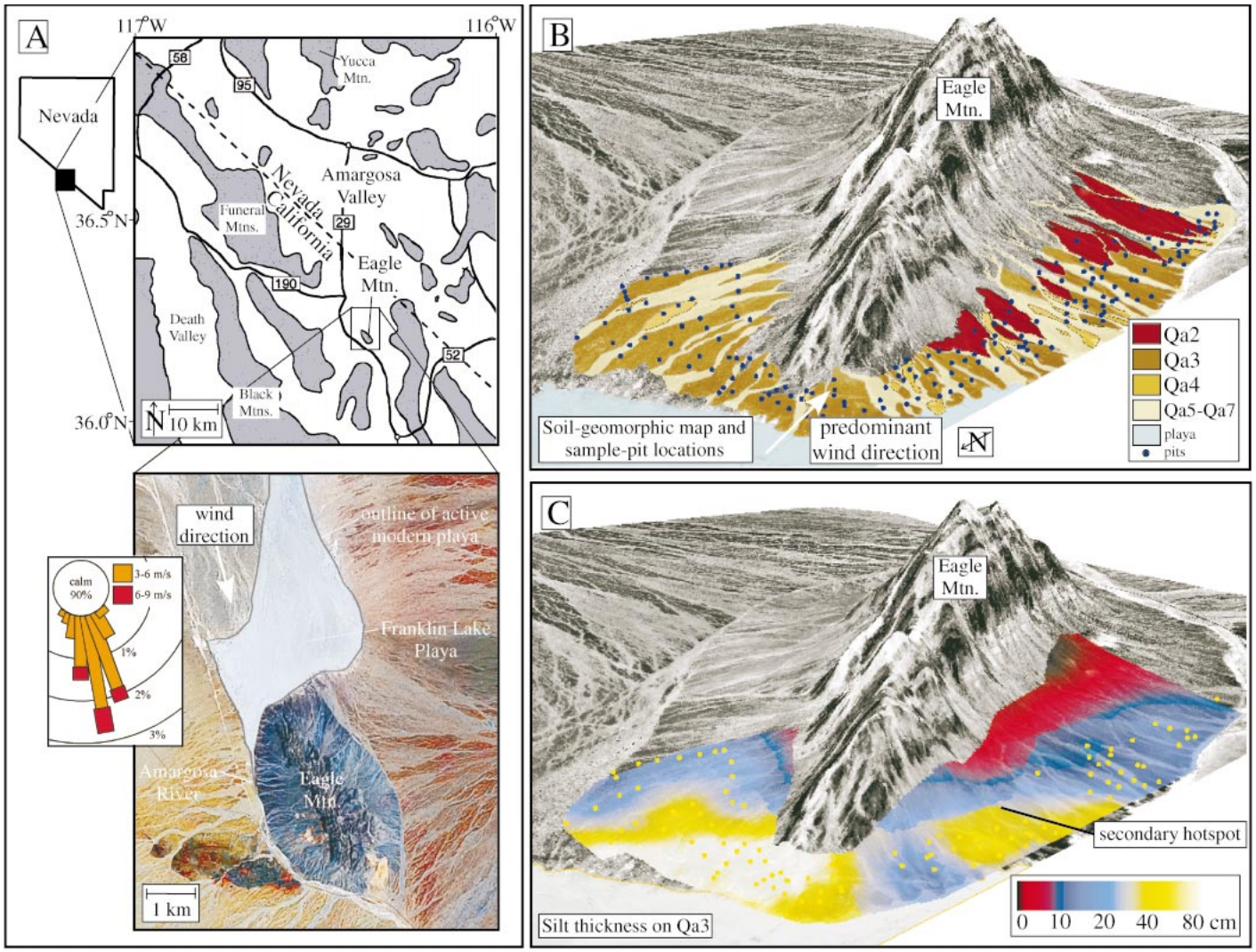

Figure 1. A: Location map and Landsat image of Eagle Mountain piedmont and adjacent Franklin Lake playa, southern Amargosa Valley, California. Predominant wind direction is SSE, as shown by wind-rose diagram (adapted from January 2003–January 2005 data from Western Regional Climate Center, 2005). Calm winds are defined to be <3 m/s. B: Soil-geomorphic map and oblique aerial perspective of Eagle Mountain piedmont, looking southeast. Terrace map units are based on regional classification by Whitney et al. (2004), discussed in Appendix DR1 (see footnote 1). Approximate ages: Qa2—middle Pleistocene, Qa3—middle to late Pleistocene, Qa4—late Pleistocene, Qa5–Qa7—latest Pleistocene to active. C: Color map of eolian silt thickness on Qa3 (middle to late Pleistocene) surface, showing maximum thicknesses of 80 cm close to playa source, decreasing by factor of ~2 for each 1 km of distance downwind. Far from playa, background values of ~20 cm were observed.

(Appendix DR1). This plot includes all measurements collected from terrace units late Pleistocene in age or older (Qa4–Qa2) within a 1-km-wide swath of western Eagle Mountain piedmont. Data from the Qa4 and Qa2 units show a similarly rapid downwind decrease in silt thickness, illustrating that the Qa3 pattern is robust. Silt thicknesses were relatively similar on the three terrace units at comparable distances from the playa. This similarity was not expected, given the great differences in age between the three surfaces. This may be partly explained by the fact that Qa2 surfaces have undergone extensive hillslope erosion (and hence preserve only a portion of the total eolian material deposited over time) and that Qa4 surfaces have received a higher average dust flux because they have existed primarily during the warm dry Holocene. The Qa5 unit (latest Pleistocene) exhibited uniformly thin deposits underlying a weak pavement, independent of distance from the playa, suggesting that the trapping ability of young surfaces is limited by weak pavement development.

NUMERICAL MODEL

Atmospheric transport of particulate matter can be modeled as a combination of turbulent diffusion, downwind advection, and gravitational settling (terms one, two, and three from left to right in equation 1). The steady-state equation describing these processes is given by

$$K\left(\frac{\partial^2 c}{\partial x^2}+\frac{\partial^2 c}{\partial y^2}+\frac{\partial^2 c}{\partial z^2}\right)-u\frac{\partial c}{\partial x}+q\frac{\partial c}{\partial z}=0, \quad (1)$$

where K is the turbulent diffusivity, c is the particle concentration, x is the downwind distance, y is the crosswind distance, z is the vertical distance from the ground, u is the mean wind velocity, and q is the settling velocity (model geometry shown in Fig. 2B). Solutions to equation 1 are known as Gaussian plumes. This version of the advection-diffusion-settling equation assumes that K and u are uniform. More complex models are also available in which K and u vary with height to better represent transport processes close to the ground (e.g., Koch, 1989; Huang, 1999).

Deposition from a Gaussian plume is modeled by treating the ground as a ''sink'' for particles. Deposition in this model is characterized by a deposition velocity, p, defined as the fraction of the particle concentration just above the ground that undergoes deposition per unit time. In this model framework, deposition at the ground surface is

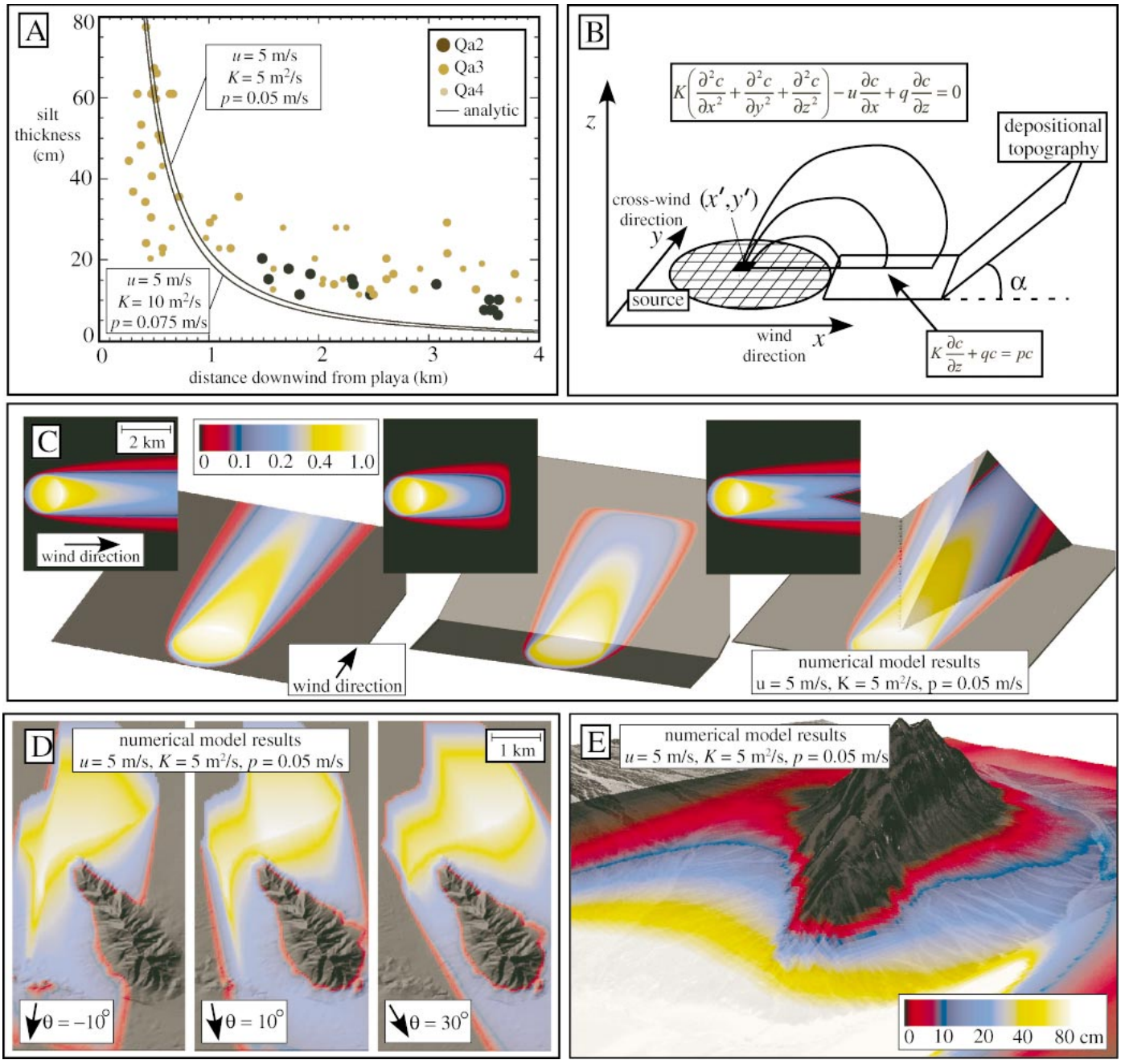

Figure 2. A: Plot of eolian silt thickness vs. downwind distance, with analytic solutions for two-dimensional model (equation DR1; see footnote 1) for representative values of model parameters. B: Schematic diagram of model geometry. Depositional topography shown in this example is inclined plane located downwind of source (but model can accept any downwind topography). C: Color maps of three-dimensional model results, illustrating role of variable downwind topography. In each case, model parameters are u = 5 m/s, K = 5 m²/s, and p = 0.05 m/s (see text). Downwind topography is, from left to right, flat plane, inclined plane, and triangular ridge. Width and depth of model domain are both 6 km. D: Color maps of three-dimensional model results for deposition downwind of Franklin Lake playa, illustrating role of variable wind direction. From left to right, wind direction is θ = −10° (0° is due south), 10°, and 30°. E: Color map of three-dimensional model results obtained by integrating model results over range of wind conditions, weighted by wind-rose data in Figure 1A.

equal to the downward flux due to turbulent diffusion and particle settling. This balance provides a flux boundary condition at $z = 0$:

$$K\frac{\partial c}{\partial z}\bigg|_{z=0} + qc(x, y, 0) = pc(x, y, 0). \quad (2)$$

Physically, the deposition velocity represents the trapping ability of the surface, independent of whether the particles are falling under gravity. Silt, for example, has a negligible settling velocity but a finite deposition velocity because silt particles are deposited as they fall or lodge between the crags of a rough surface (e.g., clasts in a desert pavement).

The three-dimensional concentration field for a point source located at $(x', y', 0)$, obtained by solving equation 1 and 2, is given by

$$c_p(x, y, z, x', y') = \frac{Q}{\sqrt{\frac{4\pi K(x - x')}{u}}} \exp\left[-\frac{u(y - y')^2}{4K(x - x')}\right]$$

$$\times \left\{ \frac{\exp\left[-\frac{uz}{4K(x-x')}\right]}{\sqrt{\pi u K(x-x')}} - \frac{p}{uK}\exp\left[\frac{pz}{K} + \frac{p^2(x-x')}{Ku}\right] \right.$$

$$\left. \cdot \operatorname{erfc}\left[\sqrt{\frac{u}{4K(x-x')}}z + p\sqrt{\frac{x-x'}{Ku}}\right] \right\}, \quad (3)$$

where Q is the source emission rate and erfc is the complementary error function. Equation 3 combines the two-dimensional solution of Smith (1962) with an additional term required to describe crosswind transport (Huang, 1999). Equation 3 assumes that the settling velocity q is small compared with the deposition velocity p. Stokes' Law (Allen, 1997) implies a settling velocity of <1 cm/s for silt particles (i.e., particles <0.05 mm) in air. Deposition velocities consistent with the spatial distribution of deposition on Eagle Mountain piedmont, however, are $\sim$5 cm/s, or at least 5 times greater than q.

For nonpoint sources, equation 3 can be integrated to give

$$c(x, y, z) = \int_{-\infty}^{\infty}\int_{-\infty}^{\infty} c_p(x', y')\, dx'\, dy'. \quad (4)$$

Using equations 3 and equations 4 , the deposition rate on a flat surface is given by $pc(x, y, 0)$. Deposition on a complex downwind surface can be estimated as $pc[x, y, h(x, y)]$, where $h(x, y)$ is the elevation of the downwind topography. This approach is only an approximation of the effects of complex topography because mass loss from the plume is still assumed to occur along a horizontal plane in equation 3. However, by using the elevated plume concentration—i.e., c[x, y, $h(x, y)$]—to estimate the deposition term pc, the model approximates the spatially variable deposition that occurs as the plume intersects with complex topography. Further model details are discussed in Appendix DR1 (see footnote 1).

Model results are shown in Figure 2C to illustrate the role of complex downwind topography in controlling deposition patterns. In each case, a circular source with uniform Q was considered with model parameters $u = 5$ m/s, $K = 5$ m^2/s, and $p = 0.05$ m/s. From left to right, the downwind topography was considered to be flat, an inclined plane, and a triangular ridge. Relative to flat topography, the inclined plane leads to a short plume, and the triangular ridge diverts and bisects the plume.

Long-term dust transport does not correspond to a single wind direction as assumed in the simplified cases of Figure 2C. The effects of multiple wind directions can be incorporated into the model by integrating a series of model runs with a range of wind directions, each weighted by the frequency of that wind direction in the wind-rose diagram. Figure 2D illustrates model results for the Eagle Mountain region with wind directions from $\theta = -10°$ to $+30°$ ($\theta = 0°$ is due south). Figure 2E illustrates the integrated model corresponding to the wind-rose diagram of Figure 1A. The thickness values mapped in Figure 2E correspond to a uniform Q value of 1.0 m/k.y. (assuming a Qa3 surface age of 50 ka), obtained by scaling the model results for different values of Q to match the maximum thickness values between the model and observed data. The modeled and observed deposition patterns match each other in most respects. However, the secondary hot spot located on the western piedmont of the study area is not reproduced by the model. This feature could result from more westerly paleowinds transporting more dust eastward from the Amargosa River relative to modern conditions. Alternatively, it could result from enhanced hillslope erosion of Qa3 surfaces in this area.

CONCLUSIONS

Numerical modeling of dust transport and deposition holds great promise for integration with classic methods in dust research. The model may be calibrated, for example, using point data from modern dust traps in order to provide a physically based regional reconstruction of dust deposition over interannual time scales (e.g., Reheis, 2003). In addition, the modeling framework may be useful for modeling sub–grid-scale processes within global-scale numerical dust-transport models.

ACKNOWLEDGMENTS

We thank Dave Miller for introducing us to this problem. Rich Reynolds, Marith Reheis, and Chris Menges provided helpful conversations on the geology of southern Amargosa Valley and dust transport in general. Peter Haff, Marith Reheis, and an anonymous reviewer provided very helpful reviews. We gratefully acknowledge support by the Army Research Office Terrestrial Sciences Program grant W911NF-04-1-0266.

REFERENCES CITED

Allen, P.A., 1997, Earth surface processes: New York, Oxford University Press, 404 p.

Bull, W.B., 1991, Geomorphic responses to climatic change: New York, Oxford University Press, 326 p.

Chadwick, O.A., and Davis, J.O., 1990, Soil-forming intervals caused by eolian sediment pulses in the Lahontan basin, northwestern Nevada: Geology, v. 18, p. 243–246, doi: 10.1130/0091-7613(1990)018<0243:SFICBE>2.3.CO;2.

Czarnecki, J.B., 1997, Geohydrology and evapotranspiration at Franklin Lake playa, Inyo County, California: U.S. Geological Survey Water-Supply Paper 2377, 75 p.

Harrison, S.P., Kohfield, K.E., Roelandt, C., and Claquin, T., 2001, The role of dust in climate changes today, at the last glacial maximum, and in the future: Earth Science Reviews, v. 54, p. 43–80, doi: 10.1016/S0012-8252(01)00041-1.

Huang, C.H., 1999, On solutions of the diffusion-deposition equation for point sources in turbulent shear flow: Journal of Applied Meteorology, v. 38, p. 250–254, doi: 10.1175/1520-0450(1999)038<0250:OSOTDD>2.0.CO;2.

Koch, W., 1989, A solution of the two-dimensional atmospheric diffusion equation with height-dependent diffusion coefficient including ground level absorption: Atmospheric Environment, v. 23, p. 1729–1732, doi: 10.1016/0004-6981(89)90057-7.

Kohfeld, K.E., Reynolds, R.L., Pelletier, J.D., and Nickling, W., 2005, Linking the scales of process, observation, and modeling of dust emissions: Eos (Transactions, American Geophysical Union), v. 86, p. 113–114.

McFadden, L.D., Wells, S.G., and Jercinovich, M.J., 1987, Influences of eolian and pedogenic processes on the origin and evolution of desert pavements: Geology, v. 15, p. 504–508, doi: 10.1130/0091-7613(1987)15<504:IOEAPP>2.0.CO;2.

McFadden, L.D., Eppes, M.C., Gillespie, A.R., and Hallet, B., 2005, Physical weathering in arid landscapes due to diurnal variation in the direction of solar heating: Geological Society of America Bulletin, v. 117, p. 161–173, doi: 10.1130/B25508.1.

Pye, K., 1987, Aeolian dust and dust deposits: London, Academic Press, 334 p.

Reheis, M.C., 2003, Dust deposition in Nevada, California, and Utah, 1984–2002: U.S. Geological Survey Open-File Report 03–138, 11p.

Reheis, M.C., Goodmacher, J.C., Harden, J.W., McFadden, L.D., Rockwell, T.K., Shroba, R.R., Sowers, J.M., and Taylor, E.M., 1995, Quaternary soils and dust deposition in southern Nevada and California: Geological Society of America Bulletin, v. 107, p. 1003–1022, doi: 10.1130/0016-7606(1995)107<1003:QSADDI>2.3.CO;2.

Samet, J.M., Dominici, F., Curriero, F.C., Cousac, I., and Zeger, S.L., 2000, Fine particulate air pollution and mortality in 20 U.S. cities, 1987–1994: New England Journal of Medicine, v. 343, p. 1742–1749, doi: 10.1056/NEJM200012143432401.

Smith, F.B., 1962, The problem of deposition in atmospheric diffusion of particulate matter: Journal of Atmospheric Sciences, v. 19, p. 429–434, doi: 10.1175/1520-0469(1962)019<0429:TPODIA>2.0.CO;2.

Watson, J.G., 2002, Visibility: Science and regulation: Air and Waste Management Association Journal, v. 52, p. 628–713.

Wells, S.G., McFadden, L.D., Poths, J., and Olinger, C.T., 1995, Cosmogenic ^{3}He surface-exposure dating of stone pavements: Implications for landscape evolution in deserts: Geology, v. 23, p. 613–616, doi: 10.1130/0091-7613(1995)023<0613:CHSEDO>2.3.CO;2.

Western Regional Climate Center, 2005, Station Wind Rose: Amargosa Valley Nevada: Desert Research Institute, http://www.wrcc.dri.edu/cgi-bin/wea_windrose.pl?nvamar (July, 2005).

Whitney, J.W., Taylor, E.M., and Wesling, J.R., 2004, Quaternary stratigraphy and mapping in the Yucca Mountain area, *in* Keefer, W.R., et al., eds., Quaternary paleoseismology and stratigraphy of the Yucca Mountain area, Nevada: U.S. Geological Survey Professional Paper 1689, p. 11–23.

Yaalon, D.H., and Ganor, E., 1973, The influence of dust on soils in the Quaternary: Soil Science, v. 116, p. 146–155.

Manuscript received 12 July 2005
Revised manuscript received 22 July 2005
Manuscript accepted 25 July 2005

Printed in USA